HHS Public Access

Author manuscript

*Bone*. Author manuscript; available in PMC 2016 December 01.

Published in final edited form as:

*Bone*. 2015 December ; 81: 370–379. doi:10.1016/j.bone.2015.07.037.

# Quantification of skeletal growth, modeling, and remodeling by *in vivo* micro computed tomography

**Allison R. Altman**[1], **Wei-Ju Tseng**[1], **Chantal M.J. de Bakker**[1], **Abhishek Chandra**[1], **Shenghui Lan**[1,2,3], **Beom Kang Huh**[1], **Shiming Luo**[1], **Mary B. Leonard**[4], **Ling Qin**[1], and **X. Sherry Liu**[1,*]

[1]McKay Orthopaedic Research Laboratory, Department of Orthopaedic Surgery, Perelman School of Medicine, University of Pennsylvania, Philadelphia, PA, United States

[2]Department of Orthopaedic Surgery, Union Hospital, Tongji Medical College, Huazhong University of Science and Technology, Hubei Province, People's Republic of China

[3]Department of Orthopaedic Surgery, Wuhan General Hospital of Guangzhou Military Command, Hubei Province, People's Republic of China

[4]Departments of Pediatrics and Medicine, Stanford University School of Medicine, Stanford, CA, United States

## Abstract

In this study we established an image analysis scheme for the investigation of cortical and trabecular bone development during skeletal growth and tested this concept on *in vivo* μCT images of rats. To evaluate its efficacy, we applied the technique to young (1-month-old) and adult (3-month-old) rat tibiae with vehicle (Veh) or intermittent parathyroid hormone (PTH) treatment. By overlaying 2 sequential scans based on their distinct trabecular microarchitecure, we calculated the linear growth rate of young rats to be 0.31 mm/day at the proximal tibia. Due to rapid growth (3.7 mm in 12 days), the scanned bone region at day 12 had no overlap with the bone tissue scanned at day 0. Instead, the imaged bone region at day 12 represented newly generated bone tissue from the growth plate. The new bone of the PTH-treated rats had significantly greater trabecular bone volume fraction, number, and thickness than those of the Veh-treated rats, indicating PTH's anabolic effect on bone modeling. In contrast, the effect of PTH on adult rat trabecular bone was found to be caused by PTH's anabolic effect on bone remodeling. The cortical bone at the proximal tibia of young rats also thickened more in the PTH group (23%) than the Veh group (14%). This was primarily driven by endosteal bone formation and coalescence of trabecular bone into the cortex. This process can be visualized by aligning the local bone structural changes using image registration. As a result, the cortex after PTH treatment was 31% less porous, and had a 22% greater polar moment of inertia compared to the Veh group. Lastly, we monitored the

*To whom correspondence should be addressed X. Sherry Liu, McKay Orthopaedic Research Laboratory, Department of Orthopaedic Surgery, University of Pennsylvania, 426C Stemmler Hall, 36th Street and Hamilton Walk, Philadelphia, PA 19104, USA, xiaoweil@mail.med.upenn.edu, Phone: 1-215-746-4668.



**Conflict of Interest:**
No authors have any conflicts of interest.

longitudinal bone growth in adult rats by measuring the distance of bone flow away from the proximal tibial growth plate from 3 months to 19 months of age and discovered a total of 3.5 mm growth in 16 months. It was demonstrated that this image analysis scheme can efficiently evaluate bone growth, bone modeling, and bone remodeling, and is ready to be translated into a clinical imaging platform.

**Keywords**

*In vivo* μCT; parathyroid hormone; trabecular coalescence; bone remodeling; endochondral bone development; bone modeling

## 1. Introduction

Diversity in adult bone size, shape, and microarchitecture is partially established in early life through bone modeling and remodeling processes during skeletal growth. Long bone growth is comprised of both types of new bone formation, either through bone modeling where the new bone matrix emerges at the growth plate through endochondral ossification, or bone remodeling where bone formation outpaces bone resorption to thicken the pre-existing bone matrix. The increase in bone mass and size through both mechanisms in young adulthood is an order of magnitude greater than the rate of bone loss in advanced age [1–4]. Thus, the factors that affect the development of cortical and trabecular bone before reaching peak bone mass may have important implications in future risk of osteoporosis and are therefore of great clinical interest.

Recent advances in clinical imaging have provided several potential means to assess the distinct structural changes in trabecular and cortical bone with maturation. By using peripheral quantitative computed tomography (pQCT) and high resolution pQCT (HR-pQCT), Wang *et al*. studied the bone structure in daughter-mother pairs and demonstrated that bone mass and size of girls at puberty correlated with those of their mothers [5]. More importantly, they performed an extensive study on the distal metaphyseal regions of long bone. In contrast to the diaphysis, which is developed primarily through periosteal apposition, the cortices of the metaphyseal region are partially derived by coalescence of trabeculae that originate from the growth plate through endochondral ossification. The HR-pQCT derived trabecular bone volume fraction of the daughters predicts both the trabecular bone morphology and cortical thickness in their mothers. In contrast, the cortical bone thickness of daughters did not predict those of their mothers [5]. Using the bone of the daughter as an indicator of the mother’s bone as a child, the above data suggest that the development of metaphyseal trabecular bone in early life is critical to the quality of both trabecular and cortical bone in adulthood.

The current available approaches to study metaphyseal bone development are limited. In clinical studies, pQCT has been used to longitudinally measure the cortical and trabecular bone size and volumetric density, and cortical thickness [6]. However, the limited slice thickness of pQCT prevents more detailed analysis of trabecular structural development and its coalescence into cortical bone. The more recently developed HR-pQCT allows longitudinal, three-dimensional (3D) imaging of both cortical and trabecular bone

microstructure [7–10]. Although prospective studies using this technology to follow the development of bone microarchitecture from childhood to adulthood are not readily available, the HR-pQCT imaging approach has great promise to provide important *in vivo* evidence of bone development with the highest temporal and spatial resolution. However, what is also not yet available is a 3D image registration scheme that can reliably follow the trabeculae from endochondral ossification through their coalescence into the cortex.

Small animal models have also been widely used to investigate the mechanisms of bone modeling and remodeling. By using *in vivo* fluorochrome labeling and dynamic bone histomorphometry in a rabbit model, it has been demonstrated that the cortices in the metaphyseal bone region are formed by trabecular coalescence during longitudinal growth [11]. Recent developments of *in vivo* μCT imaging technologies has enabled longitudinal assessment of cortical and trabecular bone structural development in rats and mice over time [12–16]. Compared to traditional 2D histology, *in vivo* μCT not only improves bone microstructure characterization by adding a spatial dimension (2D to 3D), but also provides a temporal dimension to capture the physiological processes that occur on bone, such as bone modeling and remodeling activities. However, it is challenging to obtain separate assessments of remodeling and modeling activities in animals with growth because changes in the skeleton resulting from local bone remodeling activities are often confounded with those resulting from modeling. In our recent study, we developed a 3D image registration scheme to delineate linear growth from remodeling-induced changes in the rat skeleton [16]. The primary objective of the current study was to establish an imaging and image analysis scheme for the investigation of cortical and trabecular bone development during skeletal growth based on *in vivo* high resolution microstructural imaging. We chose to test this scheme by investigating long-bone changes during growth using *in vivo* μCT on rats. This is because the ratio between the image voxel size (~10 μm) of *in vivo* μCT and rat trabecular thickness (50–100 μm) is similar to that between the image voxel size (60–80 μm) of HR-pQCT and human trabecular thickness (200–400 μm). Thus, the imaging platform developed in this study can be extended to clinical imaging applications in the near future.

To evaluate the efficacy of this imaging method for detecting responses in modeling and remodeling activity to diseases and interventions, we applied it to 1-month-old and 3-month-old rats with vehicle or intermittent parathyroid hormone (PTH) treatment and compared their responses over time. Daily PTH injections are a potent anabolic treatment for osteoporosis [17–19]. While past studies clearly demonstrate PTH's efficacy in increasing bone remodeling with a greater impact on bone formation [20–23], early studies in young rats also demonstrated a potential effect of PTH to promote bone modeling, making it an ideal candidate for testing this new image analysis scheme. We hypothesized that PTH would have a direct effect on both endochondral bone development as well as local bone remodeling in growing rats, while in contrast the response of the mature rat skeleton would be primarily due to modified local bone remodeling activities. To address this hypothesis, we used *in vivo* μCT and 3D image registration techniques to monitor the response in rat tibial bone to intermittent PTH. This investigation showed that the advanced *in vivo* imaging technique can provide direct quantification of endochondral bone modeling in the growing skeleton. Lastly, we applied the longitudinal imaging method to monitor tibial bone growth

in a group of 3-month-old rats for 16 months, demonstrating the potential of this imaging technology in studying long-term skeletal changes.

## 2. Materials and Methods

### 2.1 Animals and Treatments

Female Sprague Dawley rats (Charles River Laboratories, Wilmington, MA) were purchased for this study. Due to the minimal linear growth and low trabecular bone volume at the distal tibia (results shown in Supplemental Material), we chose the proximal tibia as the skeletal site for detailed trabecular bone imaging and analyses. Experiments were performed for 2 age groups: 1-month-old and 3-month-old rats. Within each age group, 6–8 rats were assigned in each treatment group. All experiments were approved by the University of Pennsylvania's Institutional Animal Care and Use Committee.

Both 1-month-old and 3-month-old rats were treated with daily Veh or PTH (PTH 1–34, 60μg/kg/day, Bachem, Bubendorf, Switzerland) injections for 12 days. All the rats were subjected to *in vivo* μCT scans of the proximal tibia. All rats were scanned on the first and the last day of treatment (day 0 and day 12). Our recent studies indicated that intermittent PTH treatment exerts a protective effect on bone to prevent radiation-induced bone loss in both immature and mature rats [24–26]. Therefore, in this study the PTH-treated rats were scanned additionally on days 4 and 8 during the treatment period (Figure 1). To capture the short-term bone changes in vehicle-treated 1-month-old rats, an additional 4-day experiment was performed for a separate group of 1-month old rats. These rats were treated with vehicle for 4 days and received μCT scans at day 0 and day 4 before sacrifice (Figure 1).

### 2.2 In vivo μCT Scans

Rats were anesthetized (4.0/1.75% isoflourane) and the right tibiae were scanned at 10.5 μm nominal voxel size. All the μCT scans were performed using an *in vivo* μCT system (vivaCT 40, Scanco Medical AG, Brüttisellen, Switzerland). The scanner was used at 55 kVp energy, 145 μA intensity and 200 ms integration time. Rat tibiae were immobilized by a customized holder to ensure minimal motion effect and consistent positioning during the scans [16]. Average scan time was approximately 20 minutes. A 2D scout view was used to select the scan region immediately prior to each scan, and tibia length was measured.

The proximal tibia was scanned at 10.5 μm isotropic voxel size. A reference line was placed at 0.2 mm distal to the growth plate and a total of 296 slices (corresponding to a 3.1 mm region) distal from the reference line were acquired for the 1-month-old rats. In the 3-month-old rats, a 4 mm section was selected beginning 0.2 mm distal to the growth plate. The shorter length of scan region in 1-month rats was due to the limited amount of trabecular bone in the distal region from the growth plate, as well as radiation concerns in these young, growing animals.

### 2.3 Image Registration

A landmark-initialized mutual information based registration toolkit [27, 28] of an open source software (National Library of Medicine Insight Segmentation and Registration

Toolkit, USA) [29] was used to register the baseline and follow-up scans. The registration toolkit used the mutual information metric with an implementation method specified by Viola and Wells [27]. 1% of voxels in the volume of interest were randomly selected as the spatial samples. Cubic B-Spline interpolator and quaternion rigid transform gradient descent optimizer were applied. More detailed information about the registration approach can be found in the ITK Software Guide [29]. The application of this method to evaluate longitudinal changes in rat bone have been detailed previously and resulted in improved reproducibility from unregistered bone microstructural comparisons [16]. Briefly, by registering the unaltered trabecular patterns, a common volume of trabecular bone can be located in each longitudinal μCT image so that the microstructural changes due to local bone remodeling can be quantified based on the registered trabecular volumes. Each image registration result was confirmed visually to prevent erroneous local maxima in the optimization. Due to constant linear growth and bone modeling, new cortical and trabecular bone tissue is generated under the growth plate through endochondral ossification over time. Therefore, a given trabecular bone volume of interest identified in the baseline scan will be located further away from the growth plate compared to its location at baseline (Figure 1 and 2). In addition, significant bone modeling activities occur on the cortical bone surrounding the registered trabecular volume. Endocortical bone accrual and periosteal bone resorption occur on the rat cortex to form a naturally more slender bone shape away from growth plate (Figure 1 and 2). The above physiology occurs in both young and adult rats with a much faster pace in young rats.

### 2.4 Trabecular Regions of Interest for 1-Month-Old Rats

The linear growth rate at the proximal tibia was calculated by comparing the distance over which a specified section of trabecular bone has moved, relative to the growth plate, between baseline and follow-up scans (Figure 1 and 2, details found in Supplementary Material).

Due to radiation concerns, only a 3.1 mm region of the proximal tibia was scanned for the 1-month-old rats at each time point. Because of the fast growth rate (0.31 mm/day at the proximal tibia), the region scanned at day 0 was completely out of the scanned region at day 12 (0.31 mm/day x 12 days = 3.72 mm; Figure 1). Therefore the proximal tibia was evaluated in two parts. First, the trabecular structure of the primary spongiosa (120 slices, 1.8-0.4 mm below the center of growth plate) and secondary spongiosa (150 slices, 3.3–1.8 mm below the center of growth plate) of day 0 and day 12 scans were analyzed and compared. In this comparison, day 12 scans represent newly generated bone tissue which was completely different from day 0 (Figure 1). The difference between PTH and Veh treated trabecular bone indicates the effects of altered endochondral development and bone modeling.

Next, for the PTH group and 4-day Veh group, a 1.5 mm bone segment located 0.2 mm below the growth plate at day 0 was selected and compared to the registered corresponding region in the day 4 scan (~1.5 mm below growth plate, Figure 2). By comparing the registered trabecular bone volumes, the effect of 4-days vehicle or PTH treatment driven by

local bone remodeling was delineated. These registered comparisons would indicate any altered local bone remodeling activities on the existing trabecular bone tissue.

### 2.5 Trabecular Region of Interest for 3-Month-Old Rats

For the 3-month-old rats, the linear growth rate was approximately 0.03 mm/day at the proximal tibia (Supplementary Material). Due to the much slower linear growth rate, the same VOI could be easily located in the secondary spongiosa across 12 days. Therefore, a more traditional registration scheme [16] was utilized, where a 2.4 mm bone segment of secondary spongiosa, starting 1.6 mm distal to the growth plate, was selected in each day 12 scan, and the corresponding region of interest was located in the day 0, 4, and 8 scans, by finding the optimal agreement between trabecular bone patterns of each grayscale image pair (Figure 3). By evaluating longitudinal changes in the registered trabecular bone volume, the effect of bone remodeling due to vehicle and PTH treatments can be evaluated.

### 2.6 Microstructural Analysis of Trabecular Bone

The trabecular compartment was isolated manually by a single, skilled operator and separated into either primary or secondary spongiosa VOI. Bone voxels of each VOI were segmented from bone marrow and background using a Gaussian filter (sigma = 1.2 and support = 2.0) and a global threshold corresponding to 410 mgHA/cm$^3$ for the 1-month group or 545 mgHA/cm$^3$ for the 3-month group. These thresholds were determined by an adaptive threshold function provided by the μCT image analysis software. This adaptive threshold function creates a histogram of intensities for each 3D image and identifies an optimized boundary between bone and background voxel intensities for each image. For each age group, the mean value of thresholds calculated for each image within the group was obtained as the final threshold. Bone microstructural parameters including bone volume fraction (BV/TV), trabecular thickness (Tb.Th), trabecular spacing (Tb.Sp), trabecular number (Tb.N), structure model index (SMI), connectivity density (Conn.D), and tissue mineral density (TMD) were evaluated for each VOI by 3D standard microstructural analysis provided by the μCT manufacturer. The reproducibility associated with the manual contouring of trabecular bone was assessed by two operators independently performing the procedure on 10 1-month-old rats. Precision error was 0.5–4.8% for trabecular bone measures with intra-class correlation coefficients all above 0.97.

### 2.7 Cortical Bone Analysis

A 0.5 mm section of tibial metaphyseal cortical bone, beginning 0.5 mm distal to the proximal tibia growth plate, was isolated for *in vivo* μCT images of day 0 and day 12 of both age groups. Contouring to isolate the cortical bone from the trabecular bone was performed manually by a single, skilled operator. Cortical bone was similarly filtered and segmented with a cortical bone-specific threshold corresponding to 517 mmHA/cm$^3$ for the 1-month group and 625 mmHA/cm$^3$ for the 3-month group. Again, visual confirmation of appropriate segmentation was achieved for each image. To evaluate the endochondral cortical bone expansion, periosteal (Ct.Pe.Pm) and endosteal (Ct.En.Pm) perimeters, cortical thickness (Ct.Th), porosity (Ct.Po), polar moment of inertia (Ct.pMOI), and tissue mineral density (Ct.TMD) were evaluated. The reproducibility associated with the manual contouring of

cortical bone was assessed by a single operator performing the procedure twice on 10 1-month-old rats. Precision error was 0.2–5.4% for cortical bone measures with intra-class correlation coefficients all above 0.98.

Similar analyses were performed on the diaphyseal cortical bone for 1-month-old rats to evaluate cortical bone expansion at the midshaft. A 0.5 mm cortical bone segment at 50% of the total tibia length was analyzed for day 4. The corresponding region of interest at day 8 was selected after adjusting for the proximal and distal growth over 4 days. Thus, cortical parameters were evaluated on the same region of diaphyseal cortical bone over a 4 day period.

### 2.8 The tibial growth rate over rats' life span

Six female Sprague-Dawley rats were scanned every 2–4 weeks for 16 months, starting at 3 months of age. All follow-up scans were aligned to the baseline scan through image registration, and the rate of longitudinal bone growth at the proximal tibia was calculated at each time point. Additionally, total tibial length was estimated during each scan based on a two-dimensional (2D) scout view of the whole tibia and the longitudinal growth rate of the whole tibia was derived.

### 2.9 Statistical Analysis

All the parameters were presented as mean ± standard error (SE). To evaluate the temporal changes in both the 1-month-old and 3-month-old rats, two-way, repeated-measures ANOVA were completed to investigate differences among time points and treatments for each variable of interest using NCSS 7.1.14 (NCSS, LLC, Kaysville, UT). Each comparison was covaried by its baseline value to account for initial differences between groups. Planned comparisons were made using a Bonferroni correction for multiple comparisons among time points and treatment groups. p values less than 0.05 were considered to indicate statistically significant differences or changes. All differences presented in the results are significant unless otherwise noted.

## 3. Results

### 3.1 Microstructural Analysis of Trabecular Bone

**3.1.1 Newly generated trabecular bone in 1-month-old rats—**As shown in Figure 2, linear growth and bone modeling caused significant changes in cortical bone geometry in 4 days while the major trabecular pattern remained (constant bone tissue of day 0 and day 4 highlighted in yellow). During this period of rapid bone development, the cortical bone underwent endocortical formation and periosteal resorption, forming a more slender bone shape with decreases in both periosteal and endosteal perimeters as the VOI moved towards the mid-shaft (Figure 1 and 2). Due to this rapid growth (3.7 mm in 12 days), the scanned bone region at day 12 had no overlap with the bone tissue scanned at day 0. Instead, the imaged bone section at day 12 represented newly generated bone tissue from the growth plate.

Comparing this newly generated bone tissue after 12 days of treatment to the original bone tissue at day 0, the 1-month PTH group had a significant improvement in all trabecular microstructure variables in both the primary and secondary spongiosa (all $p < 0.05$; Table 1). In comparison, no improvement in trabecular microstructure parameters was found in the Veh group at day 12 when compared to day 0. In fact, there was an increase in SMI in both primary and secondary spongiosa of Veh-treated rats, respectively. In the primary spongiosa, TMD increased by 3% over time in both groups, while TMD in the secondary spongiosa did not differ over time or between groups. The improvement due to PTH in the primary spongiosa is broadly demonstrated by the 141% greater BV/TV in the PTH treated rats compared to the Veh treated rats after 12 days. Subsequently, Tb.N and Tb.Th of the PTH group were 43% and 34% greater than those of the Veh group, respectively, and Tb.Sp was 38% less in the PTH group than the Veh group. In addition, Conn.D was 97% greater and SMI 51% lower in the PTH group, indicating a more connected and plate-like trabecular network due to intermittent PTH. Similar results were also found in the secondary spongiosa, with an even greater improvement in the PTH group than that of the Veh group (Table 1).

**3.1.2 Local trabecular bone changes in 1-month-old rats—**Trabecular microstructure parameters were evaluated for a registered trabecular bone volume in day 0 and day 4 scans to delineate the changes due to local bone remodeling (Figure 4A and C). In the Veh group, local bone remodeling led to a 45% reduction in BV/TV in 4 days, accompanied by a 42% reduction in Tb.N and a 77% increase in Tb.Sp. Moreover, Conn.D decreased by 51% and SMI increased by 8% in 4 days after Veh treatment. The only trabecular parameter which was improved was Tb.Th by 10%. In PTH-treated rats, BV/TV, Tb.N, and Conn.D reduced by 13%, 31%, and 61%, respectively, while Tb.Sp, and Tb.Th increased by 47% and 22%, respectively. There was no change in SMI after 4-day PTH treatment. When comparing 4-day changes in the Veh vs. PTH group, PTH treatment had the added benefit of significantly reducing the trabecular bone structure loss of BV/TV, Tb.N, Tb.Sp, and SMI induced by linear growth. Additionally, Tb.Th had a greater increase over 4 days in the PTH-treated vs. vehicle-treated group. TMD increased by an average of 12%, but did not differ with Veh or PTH treatment (Figure 4A).

**3.1.3 Trabecular bone in 3-month-old rats—**Minimal growth (0.03 mm/day) at the proximal tibia was observed in the adult rat group. Thus, longitudinal local trabecular changes can be tracked in a constant trabecular region over 12 days (Figure 3). Except for Tb.Th, no significant change was observed for any trabecular microstructure parameters in the vehicle-treated group. In the PTH group, BV/TV gradually increased by 7%, 18% and 32% at days 4, 8 and 12 compared to day 0. This increase in BV/TV was due to a significant increase in Tb.Th by 7%, 20%, and 35% at days 4, 8, and 12 respectively. Additionally, SMI decreased by 15% and Conn.D decreased by 19% at day 12 compared to day 0 (Figure 4B and D). In contrast, Tb.N and Tb.Sp remained constant from day 0 to 12. By day 12, Veh- and PTH-treated rats had undergone significantly different changes in BV/TV, Tb.Th, and SMI. Similar to the 1-month rats, TMD increased by 3% over 12 days but did not differ between Veh or PTH treatment groups (Figure 4B).

### 3.2 Cortical Bone Analysis

**3.2.1 Metaphyseal cortical bone in 1-month-old rats—**The effect of treatment on linear growth of cortical bone at the proximal tibial metaphysis was illustrated by day 12 and day 0 comparisons of the cortex right below the growth plate in 1-month-old rats (Figure 5 and Table 2). At day 12, the newly generated cortical bone in the Veh group had significantly greater endosteal and periosteal perimeters (Ct.En.Pm and Ct.Pe.Pm), cortical thickness (Ct.Th), porosity (Ct.Po), and polar moment of inertia (pMOI) than at day 0. Compared to the Veh group, the PTH-treated 1-month old rats had less increase in the Ct.En.Pm and Ct.Pe.Pm (16% and 23% in PTH *vs*. 30% and 28% in Veh, respectively). As a result, Ct.Th of the PTH group had a 64% increase in 12 days, which was significantly greater than the 14% increase in the Veh group. PTH treatment also reduced the increase in Ct.Po: in 12 days the Ct.Po increased by 23%, much lower than the 106% in the Veh group (Figure 5 and 6). As a result, pMOI, an indicator of cortex's resistance to bending, had a much greater increase in the PTH group (166%) than that in the Veh group (99%, Figure 5 and Table 2). Ct.TMD decreased by 2% over 12 days but did not differ between groups (Table 2).

**3.2.2 Metaphyseal cortical bone in 3-month-old rats—**The change in cortical bone over 12 days in the 3-month-old rats was much less than that in 1-month-old rats due to reduced endochondral bone modeling activities (Table 2). A 3% increase in Ct.Pe.Pm and a 17% increase in pMOI were found in the Veh group after 12 days, with no change in Ct.En.Pm, Ct.Th, or Ct.Po. In contrast, 12-day PTH treatment caused a 12% reduction in Ct.En.Pm with no change in Ct.Pe.Pm, resulting in a 26% increase in Ct.Th. Additionally, Ct.Po was reduced by 21% and pMOI was increased by 14% in the PTH group. Ct.TMD increased by 2% over 12 days but did not differ between groups (Table 2).

**3.2.3 Diaphyseal cortical bone in 1-month-old rats—**The change in diaphyseal cortical bone at the tibia midshaft was also evaluated in the 1-month-old rats. No treatment effect was found in any cortical parameter between PTH and Veh groups. Therefore, data from both treatment groups were pooled together to assess diaphyseal cortical expansion rate over 4 days. There was a 5.7% decrease in Ct.En.Pm and a trend toward a 0.6% increase ($p=0.07$) in Ct.Pe.Pm, resulting in a 12.0% increase in Ct.Th. Furthermore, there was also a 4.7% increase in pMOI, an 11.3% decrease in Ct.Po, and a 2% increase in Ct.TMD.

### 3.3 Tibial growth rate throughout rats' life-span

Between the ages of 3 and 19 months, the trabecular bone below the growth plate flowed towards the midshaft by a distance of 3.5 mm. The total tibia growth rate of (based on 2D scout view x-rays) and that of the proximal metaphasis (based on 3D image registration) was reported in Figure 7. Between 4 and 13 months, the distance of growth of the total tibia was significantly higher than that of the proximal tibia. Nevertheless, the distance of growth from the proximal tibia accounted for more than 80% of the total tibia growth. The growth rate of 1-month-old rats was significantly higher than that of 3-month-old rats. There was a growth spurt at the age of 4 months as indicated by both total tibial growth rate and the proximal tibial growth rate. As rats continued to age, the growth rate further slowed down and reached a plateau around 6 months of age (Figure 7).

## Discussion

In this study we developed and tested a novel *in vivo* imaging technique for studying skeletal growth, modeling, and remodeling. By using this technique, we thoroughly characterized both cortical and trabecular bone changes during endochondral ossification in growing rats in a 3-dimensional and longitudinal manner. Based on advanced image registration techniques and analysis, we were able to capture 3D longitudinal bone structure with the highest possible spatial resolution (voxel size = 10.5 μm) and temporal resolution (4 days for PTH-treated rats). In addition, we delineated the changes due to local dynamics (bone remodeling) from those due to linear growth (bone modeling), and further demonstrated the distinct skeletal structural responses in bone modeling and remodeling of young versus adult rats to intermittent PTH. Finally, we monitored a group of 3-month-old rats for 16 months and obtained an in-depth understanding of the rats' skeletal physiology across its life span.

Three-dimensional skeletal growth patterns were studied using 1-month-old rats whose skeletal structure still undergoes drastic changes due to rapid linear growth and endochondral bone development. As illustrated by longitudinal μCT images, more than 3 mm of new bone was generated from the growth plate in only 12 days (Figure 1). During natural growth (as demonstrated by the Veh-treated group over 12 days), trabecular bone properties in the newly generated primary and secondary spongiosa remained constant (Table 1) while the endosteal and periosteal surfaces of metaphyseal cortical bone underwent significant expansion (Figure 5 and Table 2). To differentiate the effect of bone remodeling during the endochondral ossification process, a registered trabecular bone segment located between the primary and secondary spongiosa at day 0 was translated to the secondary spongiosa at day 4 (Figure 2). During this transition, the trabecular volume and number decreased while trabeculae became thickened (Figure 4A). This is supported by previous histological studies detailing the transference of trabecular bone away from the growth plate and eventually into the cortical bone [11, 30].

When intermittent PTH was administered to 1-month-old rats, the trabecular bone quality of the primary spongiosa was significantly improved. PTH treatment also caused a significant increase in the width of the hypertrophic zone of the growth plate as shown by histological analysis (Supplemental Figure 1) [31, 32]. Moreover, the present work identified an increase in bone spicule thickness from the growth plate in PTH treated rats, despite no difference in chondrocyte columns or the number of bone spicules in the primary spongiosa. This ultimately resulted in more trabecular coalescence in the primary spongiosa, leading to thicker, more well defined trabecular structures in the secondary spongiosa and thicker metaphyseal cortical bone (Supplemental Figure 1). Previous studies have demonstrated the critical role of PTH, PTHrP, and PTH/PTHrP receptors in regulating postnatal bone development [32–37]. We suspect that intermittent PTH may play a role in chondrocyte hypertrophy and calcification, resulting in greater mineral density and improved structure in the primary spongiosa. This improvement in the primary spongiosa is one of two major causes leading to significantly greater trabecular bone volume and structure of the secondary spongiosa in response to PTH treatment. The second cause of improved trabecular bone quality in the secondary spongiosa was stimulated local bone formation. PTH increased the osteoblast surface on the trabecular bone (Supplemental Table 1) and protected trabecular

volume and number from bone loss during the transition from primary spongiosa to secondary spongiosa. In the meantime, greater trabecular thickening during the transition in the PTH group versus the Veh group also indicated increased local bone formation due to PTH treatment.

In adult rats, the endochondral bone development process was much slower and thus the effects of bone modeling were minimal compared to the rapidly growing younger rats. PTH increased trabecular bone mass in adult rats by thickening the existing trabeculae. This can be explained by significantly increased osteoblast number and surface (Supplemental Table 1), and was also suggested by previous studies [20–22, 38]. Thus, we conclude that the young and adult rat responses to PTH are not directly comparable due to their distinct bone structural development mechanisms.

In the growing, 1-month-old rat skeleton, the porosity in the diaphyseal cortex of the tibia shaft decreased from 9% to 8% in 4 days. The diaphyseal cortex thickness increased, primarily through formation on the endosteal bone surface, with less significant expansion of the periosteal bone surface. In contrast, the porosity in the metaphyseal cortex of the proximal tibia increased from 14% to 27% in 12 days during skeletal growth. However, this increase is transient as in the 3-month old rats the metaphysial cortical porosity had decreased to 9% and remained constant over 12 days (Table 2). These intriguing observations are consistent with a clinical report that there is a transient increase in intracortical porosity during pubertal growth spurts [39]. As suggested by Wang and Seeman [40], the mechanism responsible for increased porosity is the condensation of trabeculae. An earlier study by Cadet *et al*. examined the longitudinal development of cortical bone in rabbits by dynamic bone histomorphometry and demonstrated that the cortices in the metaphyseal region are formed by trabecular coalescence leaving unfilled pores between trabeculae during rapid growth [11]. Indeed, by using a registered *in vivo* μCT imaging technique, we acquired direct evidence of trabecular condensation at the metaphyseal cortex of rat tibia. As shown in Figure 6, rapid growth leads to endocortical surface coalescence and periosteal resorption, which produces more unfilled pores in the cortex. Furthermore, by treating young rats with intermittent PTH, we observed reduced expansion in both metaphyseal periosteal and endosteal perimeters, indicating reduced periosteal formation and endosteal resorption. It is likely that PTH also stimulated greater endosteal trabecular consolidation by improved bone formation, as cortical thickness was greater and porosity lower than the Veh group following 12-days of treatment. Although the circumference of PTH-treated bone was smaller than that of the Veh-treated bone, thicker cortex and lower porosity led to a greater polar moment of inertia, indicating greater mechanical competence of the metaphyseal cortex in protecting bone from bending. Interestingly, we did not find any difference between the effect of PTH and Veh on diaphyseal cortical expansion, suggesting the treatment effect of PTH on cortical bone is site-specific.

Intrigued by unceasing endochondral ossification in rats, we monitored the longitudinal bone growth by measuring the distance of bone flow away from the proximal tibial growth plate from the age of 3 months to 19 months. Although adult rats have a much slower growth rate compared to 1-month old rats, there was a total of 3.5 mm of growth in 16 months. A typical μCT scan of rat tibia bone consists of a 4 mm region of the secondary

spongiosa. Therefore, it should be taken into consideration in studies that are designed to examine long-term effects on bone that the observed secondary spongiosa bone quality may result from linear growth and bone modeling, in addition to bone remodeling.

There were limitations associated with this study. First, there was ionizing radiation involved with each *in vivo* μCT scan. The possible radiation damage to bone through *in vivo* μCT scans has been well recognized as several studies investigated the risk and proposed imaging protocols that minimize such damage [41–43]. These studies have shown that rat bone was less sensitive to radiation than mouse bone and a weekly scan regime has a minimal effect on bone structure and bone marrow cells [41–43]. Based on our previous study we adapted different protocols based on animal age and treatment group [24, 44]. By comparing the radiated and contralateral non-radiated tibiae, we confirmed that the effect of radiation on the tibial bone is minimal compared to the changes due to linear growth or PTH treatment (data not shown). Thus, we consider the radiation effect in our experiments to be negligible and expect that it would not alter the conclusions of the study. Second, due to little or no Haversian remodeling and continuous endochondral formation into adulthood, a rat model may not be the most appropriate model to study aging in cortical bone [45, 46]. However, the metaphyseal cortical bone development of 1-month-old rats is driven by endochondral bone formation and coalescence of trabecular bone to cortical bone. Such mechanisms are similar to cortical bone development during a human pubertal growth spurt [39, 40], thus justifying the use of a growing rat model to study the response to PTH in adolescence. However, it should be noted that our findings in the young and adult rat skeleton, especially in cortical bone, cannot necessarily be applied to aged bone. Additionally, clinical reports of PTH treatment have shown increased cortical porosity, which was not found in the present study. The major cause of increased porosity in aged humans is the imbalanced remodeling of Haversian canals [47]; such a mechanism cannot be studied using the rat model due to its lack of Haversian bone [45, 46]. Lastly, while the dose of PTH administered in this study has been show to be effective in young rats [24, 44], it far exceeds the recommended clinical dose in humans. As such, these results should be further confirmed in a clinical model before being applied to human populations.

Despite the above limitations, our study also has several notable strengths. Advanced *in vivo* imaging and image registration techniques enable us to directly quantify the influence of linear growth and local bone remodeling on trabecular bone microstructure. This longitudinal imaging strategy not only reduced the number of animals and increased the statistical power but also added a temporal dimension to the experiment. This technique is especially pertinent in the bone research field, as it allows us to directly visualize many biological processes over time. In contrast, traditional methods can only infer changes over time based on cross sectional comparisons or fluorescent labeling in dynamic histomorphometry. Most importantly, this technique can be translated to clinical imaging platforms, such as HR-pQCT imaging or micro magnetic resonance imaging (μMRI), for longitudinal evaluation of bone growth, modeling, and remodeling.

In summary, a longitudinal imaging and image registration technique was developed and its efficacy for distinguishing the skeletal response to bone modeling and remodeling was showcased in this study. By applying this technique to *in vivo* images of young rats with

PTH treatment, we demonstrated that in addition to the anabolic effect on local bone remodeling, PTH may have a direct effect on endochondral bone development in the growing skeleton. Additionally, the efficacy of the imaging technique for long-term follow-up evaluation of skeletal growth was illustrated by monitoring a group of adult rats over 16 months. We expect this novel image registration technique to be translated to clinical imaging platforms in the near future and to provide a more efficient, longitudinal evaluation of bone growth, modeling, and remodeling.

## Supplementary Material

Refer to Web version on PubMed Central for supplementary material.

## Acknowledgements

This study was supported by the McCabe Pilot Award (to XSL), NIH/NIAMS R03-AR065145 (to XSL), NIH/NIAMST32-AR007132 (to CMJdB), the National Science Foundation Graduate Research Fellowship (to CMJdB), NIH/NIDDK R01-DK09580301 (to LQ), and Penn Center for Musculoskeletal Disorders (NIH/NIAMS P30-AR050950).

## References

1. Wang Q, Seeman E. Skeletal growth and peak bone strength. Best Pract Res Clin Endocrinol Metab. 2008; 22:687–700. [PubMed: 19028352]
2. Wang Q, Cheng S, Alen M, Seeman E. Bone's structural diversity in adult females is established before puberty. J Clin Endocrinol Metab. 2009; 94:1555–1561. [PubMed: 19223517]
3. Loro ML, Sayre J, Roe TF, Goran MI, Kaufman FR, Gilsanz V. Early identification of children predisposed to low peak bone mass and osteoporosis later in life. J Clin Endocrinol Metab. 2000; 85:3908–3918. [PubMed: 11061556]
4. Hui SL, Slemenda CW, Johnston CC Jr. The contribution of bone loss to postmenopausal osteoporosis. Osteoporos Int. 1990; 1:30–34. [PubMed: 2133638]
5. Wang Q, Ghasem-Zadeh A, Wang XF, Iuliano-Burns S, Seeman E. Trabecular bone of growth plate origin influences both trabecular and cortical morphology in adulthood. J Bone Miner Res. 2011; 26:1577–1583. [PubMed: 21312271]
6. Zemel BS. Quantitative computed tomography and computed tomography in children. Curr Osteoporos Rep. 2011; 9:284–290. [PubMed: 21968815]
7. Boutroy S, Bouxsein ML, Munoz F, Delmas PD. In vivo assessment of trabecular bone microarchitecture by high-resolution peripheral quantitative computed tomography. J Clin Endocrinol Metab. 2005; 90:6508–6515. [PubMed: 16189253]
8. Liu XS, Zhang XH, Sekhon KK, Adams MF, McMahon DJ, Bilezikian JP, Shane E, Guo XE. High-resolution peripheral quantitative computed tomography can assess microstructural and mechanical properties of human distal tibial bone. J Bone Miner Res. 2010; 25:746–756. [PubMed: 19775199]
9. MacNeil JA, Boyd SK. Accuracy of high-resolution peripheral quantitative computed tomography for measurement of bone quality. Med Eng Phys. 2007; 29:1096–1105. [PubMed: 17229586]
10. Burghardt AJ, Kazakia GJ, Sode M, de Papp AE, Link TM, Majumdar S. A longitudinal HR-pQCT study of alendronate treatment in postmenopausal women with low bone density: Relations among density, cortical and trabecular microarchitecture, biomechanics, and bone turnover. J Bone Miner Res. 2010; 25:2558–2571. [PubMed: 20564242]
11. Cadet ER, Gafni RI, McCarthy EF, McCray DR, Bacher JD, Barnes KM, Baron J. Mechanisms responsible for longitudinal growth of the cortex: coalescence of trabecular bone into cortical bone. J Bone Joint Surg Am. 2003; 85-A:1739–1748. [PubMed: 12954833]
12. Boyd SK, Davison P, Muller R, Gasser JA. Monitoring individual morphological changes over time in ovariectomized rats by in vivo micro-computed tomography. Bone. 2006; 39:854–862. [PubMed: 16757220]

13. Waarsing JH, Day JS, van der Linden JC, Ederveen AG, Spanjers C, De Clerck N, Sasov A, Verhaar JA, Weinans H. Detecting and tracking local changes in the tibiae of individual rats: a novel method to analyse longitudinal in vivo micro-CT data. Bone. 2004; 34:163–169. [PubMed: 14751574]
14. Brouwers JE, Lambers FM, van Rietbergen B, Ito K, Huiskes R. Comparison of bone loss induced by ovariectomy and neurectomy in rats analyzed by in vivo micro-CT. J Orthop Res. 2009; 27:1521–1527. [PubMed: 19437511]
15. Schulte FA, Lambers FM, Kuhn G, Muller R. In vivo micro-computed tomography allows direct three-dimensional quantification of both bone formation and bone resorption parameters using time-lapsed imaging. Bone. 2011; 48:433–442. [PubMed: 20950723]
16. Lan S, Luo S, Huh BK, Chandra A, Altman AR, Qin L, Liu XS. 3D image registration is critical to ensure accurate detection of longitudinal changes in trabecular bone density, microstructure, and stiffness measurements in rat tibiae by in vivo micro computed tomography (μCT). Bone. 2013; 56:83–90. [PubMed: 23727434]
17. Lindsay R, Nieves J, Formica C, Henneman E, Woelfert L, Shen V, Dempster D, Cosman F. Randomised controlled study of effect of parathyroid hormone on vertebral-bone mass and fracture incidence among postmenopausal women on oestrogen with osteoporosis. Lancet. 1997; 350:550–555. [PubMed: 9284777]
18. Greenspan SL, Bone HG, Ettinger MP, Hanley DA, Lindsay R, Zanchetta JR, Blosch CM, Mathisen AL, Morris SA, Marriott TB. Effect of recombinant human parathyroid hormone (1–84) on vertebral fracture and bone mineral density in postmenopausal women with osteoporosis: a randomized trial. Ann Intern Med. 2007; 146:326–339. [PubMed: 17339618]
19. Neer RM, Arnaud CD, Zanchetta JR, Prince R, Gaich GA, Reginster JY, Hodsman AB, Eriksen EF, Ish-Shalom S, Genant HK, Wang O, Mitlak BH. Effect of parathyroid hormone (1–34) on fractures and bone mineral density in postmenopausal women with osteoporosis. N Engl J Med. 2001; 344:1434–1441. [PubMed: 11346808]
20. Qin L, Raggatt LJ, Partridge NC. Parathyroid hormone: a double-edged sword for bone metabolism. Trends Endocrinol Metab. 2004; 15:60–65. [PubMed: 15036251]
21. Goltzman D. Studies on the mechanisms of the skeletal anabolic action of endogenous and exogenous parathyroid hormone. Arch Biochem Biophys. 2008; 473:218–224. [PubMed: 18358824]
22. Datta NS, Abou-Samra AB. PTH and PTHrP signaling in osteoblasts. Cell Signal. 2009; 21:1245–1254. [PubMed: 19249350]
23. Jilka RL. Molecular and cellular mechanisms of the anabolic effect of intermittent PTH. Bone. 2007; 40:1434–1446. [PubMed: 17517365]
24. Chandra A, Lan S, Zhu J, Lin T, Zhang X, Siclari VA, Altman AR, Cengel KA, Liu XS, Qin L. PTH prevents the adverse effects of focal radiation on bone architecture in young rats. Bone. 2013; 55:449–457. [PubMed: 23466454]
25. Chandra A, Lin T, Tribble MB, Zhu J, Altman AR, Tseng WJ, Zhang Y, Akintoye SO, Cengel K, Liu XS, Qin L. PTH1-34 alleviates radiotherapy-induced local bone loss by improving osteoblast and osteocyte survival. Bone. 2014; 67:33–40. [PubMed: 24998454]
26. Chandra A, Lin T, Zhu J, Tong W, Huo Y, Jia H, Zhang Y, Liu XS, Cengel K, Xia B, Qin L. PTH1-34 Blocks Radiation-induced Osteoblast Apoptosis by Enhancing DNA Repair through Canonical Wnt Pathway. J Biol Chem. 2015; 290:157–167. [PubMed: 25336648]
27. Viola P, Wells WM III. Alignment by maximization of mutual information. Int J Comput Vis. 1997; 24:137–154.
28. Collignon, A.; Maes, F.; Delaere, D.; Vandermeulen, D.; Suetens, P.; Marchal, G. Automated multi-modality image registration based on information theory. In: Bizais, Y.; Barillot, C.; di Paola, R., editors. Information Processing in Medical Imaging. Dordrecht, The Netherlands: Kluwer Academic Publishers; 1995. p. 263-274.
29. Ibanez, L.; Schroeder, W.; Ng, L.; Cates, J. [Accessed December 5, 2008] The ITK Software Guide. 2nd Ed.Available at http://www.itk.org/ItkSoftwareGuide.pdf.
30. Rauch F. The dynamics of bone structure development during pubertal growth. J Musculoskelet Neuronal Interact. 2012; 12:1–6. [PubMed: 22373945]

31. Lim SK, Won YJ, Park DH, Shin DH, Yook JI, Lee HC, Huh KB. Intermittent parathyroid hormone treatment can promote linear growth in the ovariectomized growing rat. Yonsei Med J. 1999; 40:166–172. [PubMed: 10333721]
32. Demiralp B, Chen HL, Koh AJ, Keller ET, McCauley LK. Anabolic actions of parathyroid hormone during bone growth are dependent on c-fos. Endocrinology. 2002; 143:4038–4047. [PubMed: 12239115]
33. Schipani E, Provot S. PTHrP, PTH, and the PTH/PTHrP receptor in endochondral bone development. Birth Defects Res C Embryo Today. 2003; 69:352–362. [PubMed: 14745975]
34. Xue Y, Karaplis AC, Hendy GN, Goltzman D, Miao D. Genetic models show that parathyroid hormone and 1,25-dihydroxyvitamin D3 play distinct and synergistic roles in postnatal mineral ion homeostasis and skeletal development. Hum Mol Genet. 2005; 14:1515–1528. [PubMed: 15843402]
35. Iwamoto M, Jikko A, Murakami H, Shimazu A, Nakashima K, Iwamoto M, Takigawa M, Baba H, Suzuki F, Kato Y. Changes in parathyroid hormone receptors during chondrocyte cytodifferentiation. J Biol Chem. 1994; 269:17245–17251. [PubMed: 8006032]
36. Xue Y, Zhang Z, Karaplis AC, Hendy GN, Goltzman D, Miao D. Exogenous PTH-related protein and PTH improve mineral and skeletal status in 25-hydroxyvitamin D-1alpha-hydroxylase and PTH double knockout mice. J Bone Miner Res. 2005; 20:1766–1777. [PubMed: 16160734]
37. Hirai T, Chagin AS, Kobayashi T, Mackem S, Kronenberg HM. Parathyroid hormone/parathyroid hormone-related protein receptor signaling is required for maintenance of the growth plate in postnatal life. Proc Natl Acad Sci U S A. 2011; 108:191–196. [PubMed: 21173257]
38. Chiavistelli S, Giustina A, Mazziotti G. Parathyroid hormone pulsatility: physiological and clinical aspects. Bone Res. 2015; 3:14049. [PubMed: 26273533]
39. Kirmani S, Christen D, van Lenthe GH, Fischer PR, Bouxsein ML, McCready LK, Melton LJ 3rd, Riggs BL, Amin S, Muller R, Khosla S. Bone structure at the distal radius during adolescent growth. J Bone Miner Res. 2009; 24:1033–1042. [PubMed: 19113916]
40. Seeman E, Wang Q. Growth-related cortical fragility at metaphyseal regions. IBMS BoneKEy. 2009; 6:429–433.
41. Brouwers JE, van Rietbergen B, Huiskes R. No effects of in vivo micro-CT radiation on structural parameters and bone marrow cells in proximal tibia of wistar rats detected after eight weekly scans. J Orthop Res. 2007; 25:1325–1332. [PubMed: 17568420]
42. Klinck RJ, Campbell GM, Boyd SK. Radiation effects on bone architecture in mice and rats resulting from in vivo micro-computed tomography scanning. Med Eng Phys. 2008; 30:888–895. [PubMed: 18249025]
43. Laperre K, Depypere M, van Gastel N, Torrekens S, Moermans K, Bogaerts R, Maes F, Carmeliet G. Development of micro-CT protocols for in vivo follow-up of mouse bone architecture without major radiation side effects. Bone. 2011; 49:613–622. [PubMed: 21763477]
44. Altman AR, Tseng WJ, de Bakker CM, Huh BK, Chandra A, Qin L, Liu XS. A closer look at the immediate trabecula response to combined parathyroid hormone and alendronate treatment. Bone. 2014; 61C:149–157. [PubMed: 24468717]
45. Bach-Gansmo FL, Irvine SC, Bruel A, Thomsen JS, Birkedal H. Calcified cartilage islands in rat cortical bone. Calcif Tissue Int. 2013; 92:330–338. [PubMed: 23274728]
46. Shipov A, Zaslansky P, Riesemeier H, Segev G, Atkins A, Shahar R. Unremodeled endochondral bone is a major architectural component of the cortical bone of the rat (Rattus norvegicus). J Struct Biol. 2013; 183:132–140. [PubMed: 23643909]
47. Seeman E. Age- and menopause-related bone loss compromise cortical and trabecular microstructure. J Gerontol A Biol Sci Med Sci. 2013; 68:1218–1225. [PubMed: 23833200]
48. Parfitt AM, Drezner MK, Glorieux FH, Kanis JA, Malluche H, Meunier PJ, Ott SM, Recker RR. Bone histomorphometry: standardization of nomenclature symbols units. Report of the ASBMR Histomorphometry Nomenclature Committee. J Bone Miner Res. 1987; 2:595–610. [PubMed: 3455637]
49. Zhang X, Siclari VA, Lan S, Zhu J, Koyama E, Dupuis HL, Enomoto-Iwamoto M, Beier F, Qin L. The critical role of the epidermal growth factor receptor in endochondral ossification. J Bone Miner Res. 2011; 26:2622–2633. [PubMed: 21887704]

## Highlights

- A novel, *in vivo* μCT-based imaging and registration technique was developed and tested for studying skeletal growth, modeling, and remodeling.
- The efficacy was demonstrated by delineating PTH-mediated improvements in bone remodeling from those through endochondral ossification in growing rats.
- This new technique monitors endosteal bone formation and coalescence of trabeculae into the cortex in the growing skeleton.
- 3-month-old rats were monitored for 16 months by this technique, demonstrating its potential for monitoring long-term skeletal changes.

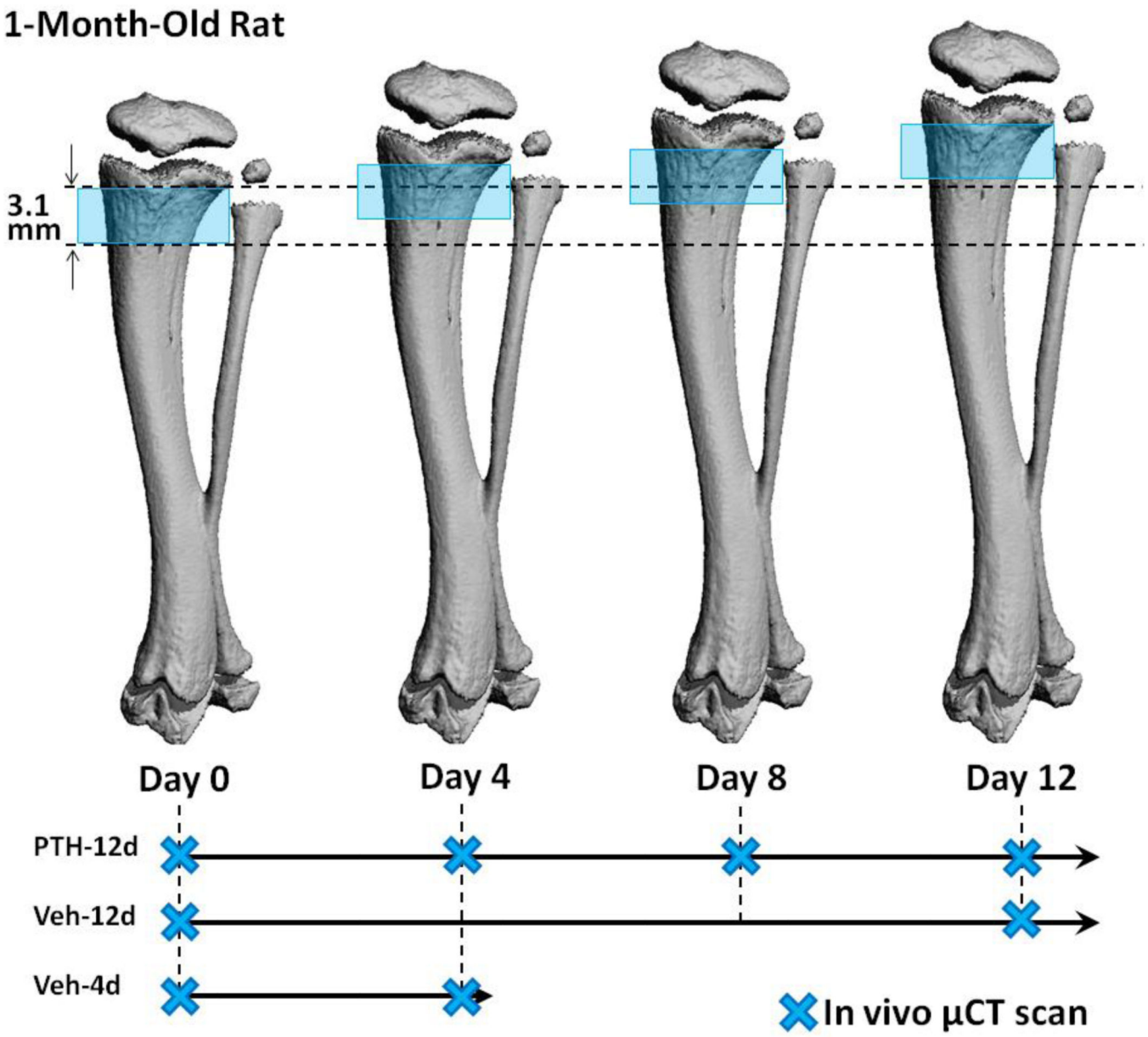


**Figure 1.**

A schematic of the study design demonstrating the relationship between µCT scanned regions and linear growth in a 1-month-old rat tibia over 12 days. The blue shade indicates the region scanned at each time point. The region between the two dotted lines indicates the bone tissue that was scanned at day 0. The relative position of the imaged bone region at day 0 becomes further away from the growth plate due to linear growth at day 4, 8, and 12.

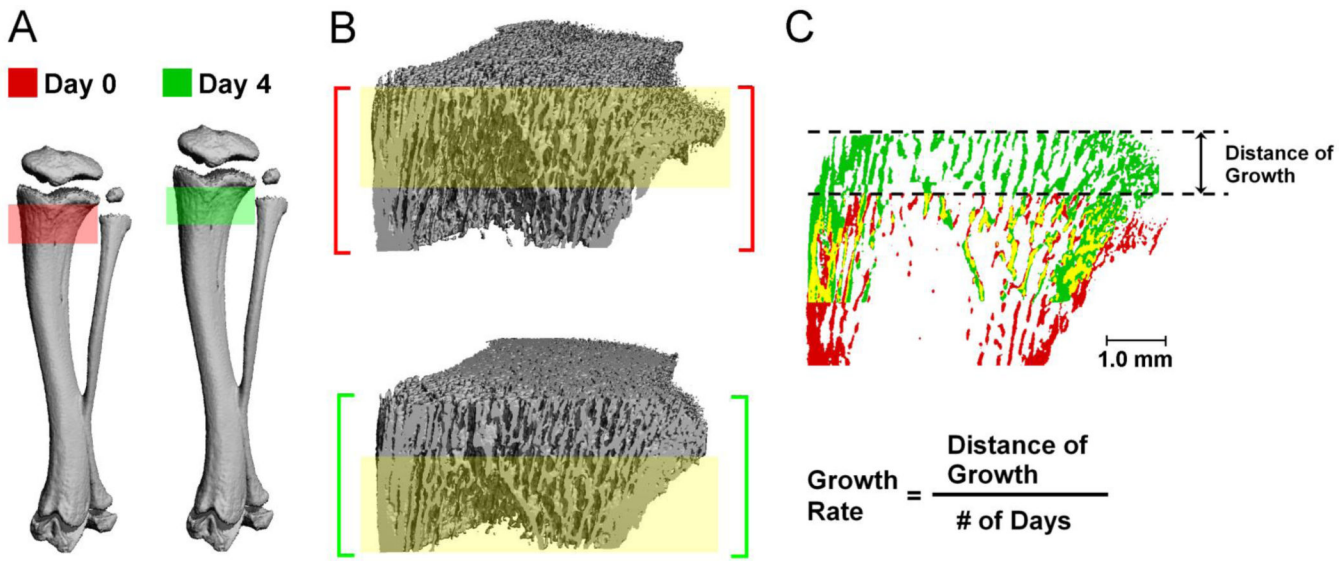


**Figure 2.**

(A) 3D bone structure of a 1-month-old PTH-treated rat proximal tibia at day 0 (red) and day 4 (green); (B) Registered common bone regions between day 0 and day 4 scans are highlighted by the yellow shaded rectangle; (C) Overlayed longitudinal 2D view of registered bone structure images of day 0 (red) and day 4 (green), where bone present in both images is shown in yellow. Growth rate is calculated as the distance of growth divided by the number of days.

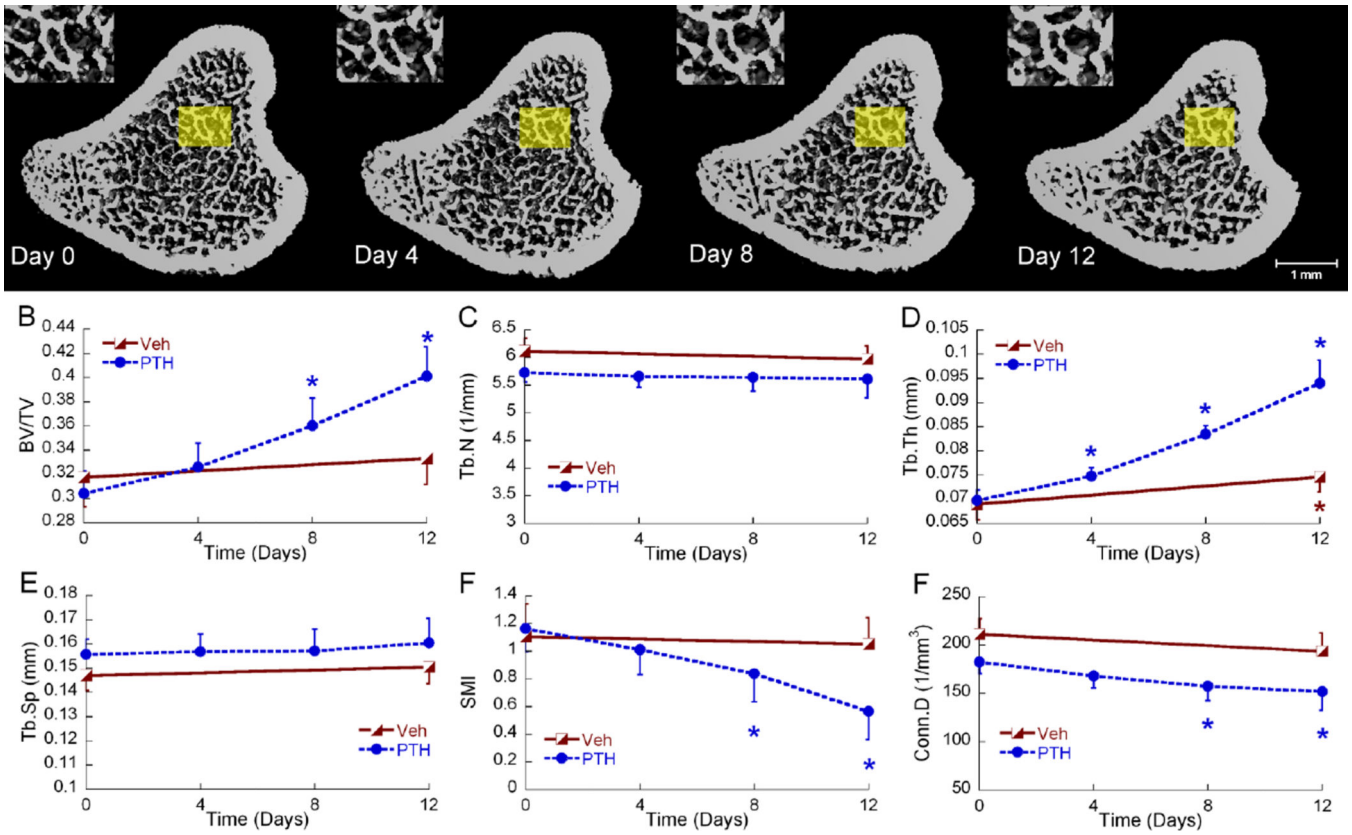


**Figure 3.**

(A) 3D bone structure of a represntative 3-month-old PTH treated rat proximal tibia at day 0, 4, 8, and 12. For illustration purposes, similar trabecular patterns are enlarged in the insets. (B–F) Longitudinal changes in registered trabecular bone microstructure parameters of 3-month-old rats in response to Veh and PTH represented as mean±SEM. Blue and red asterisks indicate significant differences from day 0.

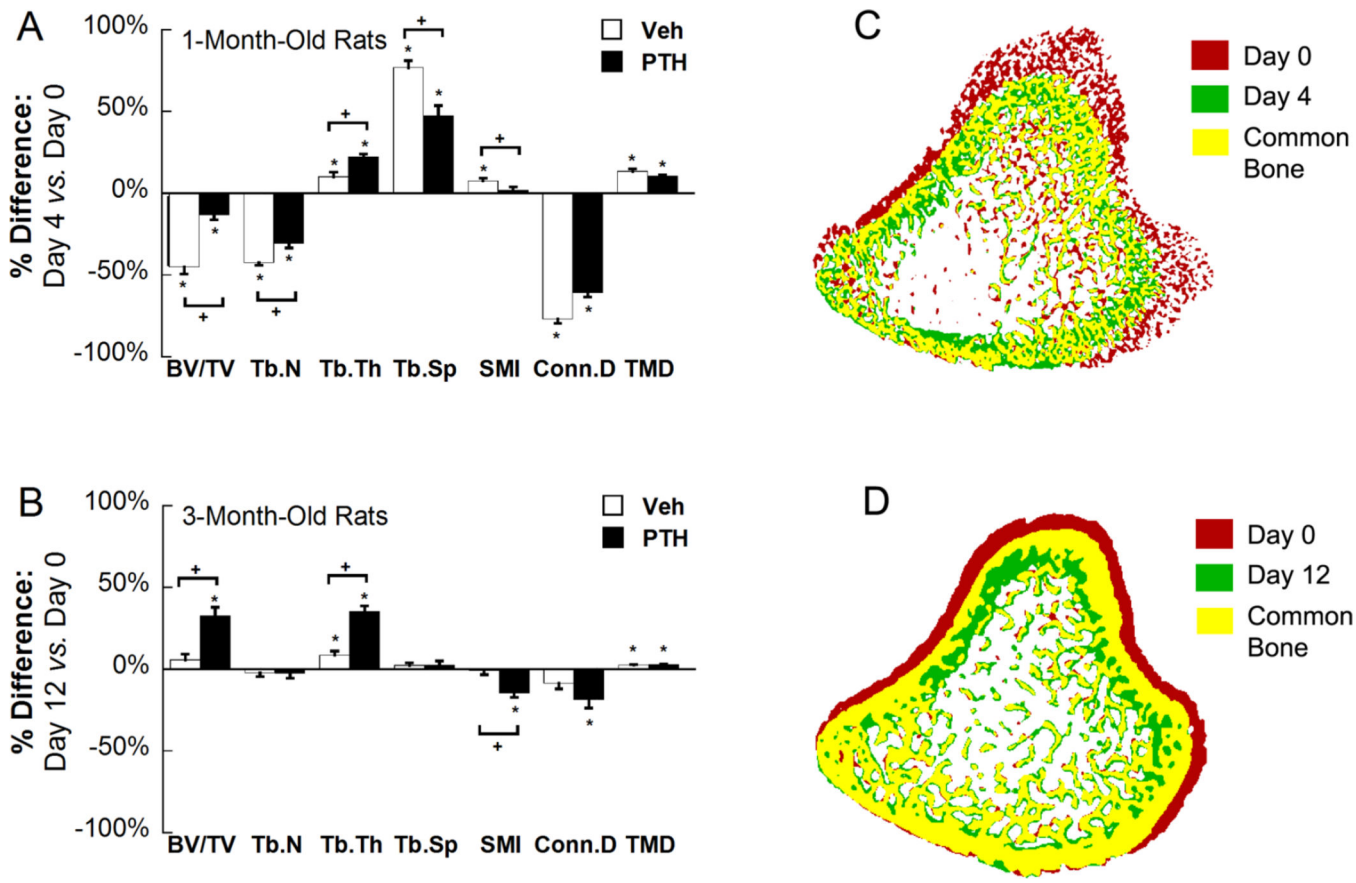


**Figure 4.**

(A) Percent difference between registered trabecular bone at day 0 and day 4 in 1-month-old Veh and PTH treated rats. (B) Percent difference between registered trabecular bone at day 0 and day 12 in 3-month-old Veh and PTH treated rats. Registered bone tissue of baseline and follow-up scans were evaluated in the above comparisons. Values represented as mean change over time±SEM, * indicates significant change from day 0; + indicates significant difference between changes in Veh and PTH groups. (C) Top view of overlaid bone images of day 0 and day 4 of 1-month-old PTH-treated rats and (D) day 0 and day 12 of 3-month-old PTH treated rats. Red indicates bone tissue that only exists at day 0; green indicates bone tissue that only exists at day 4 (day 12); yellow indicates bone tissue that exists at both day 0 and day 4 (day 12).

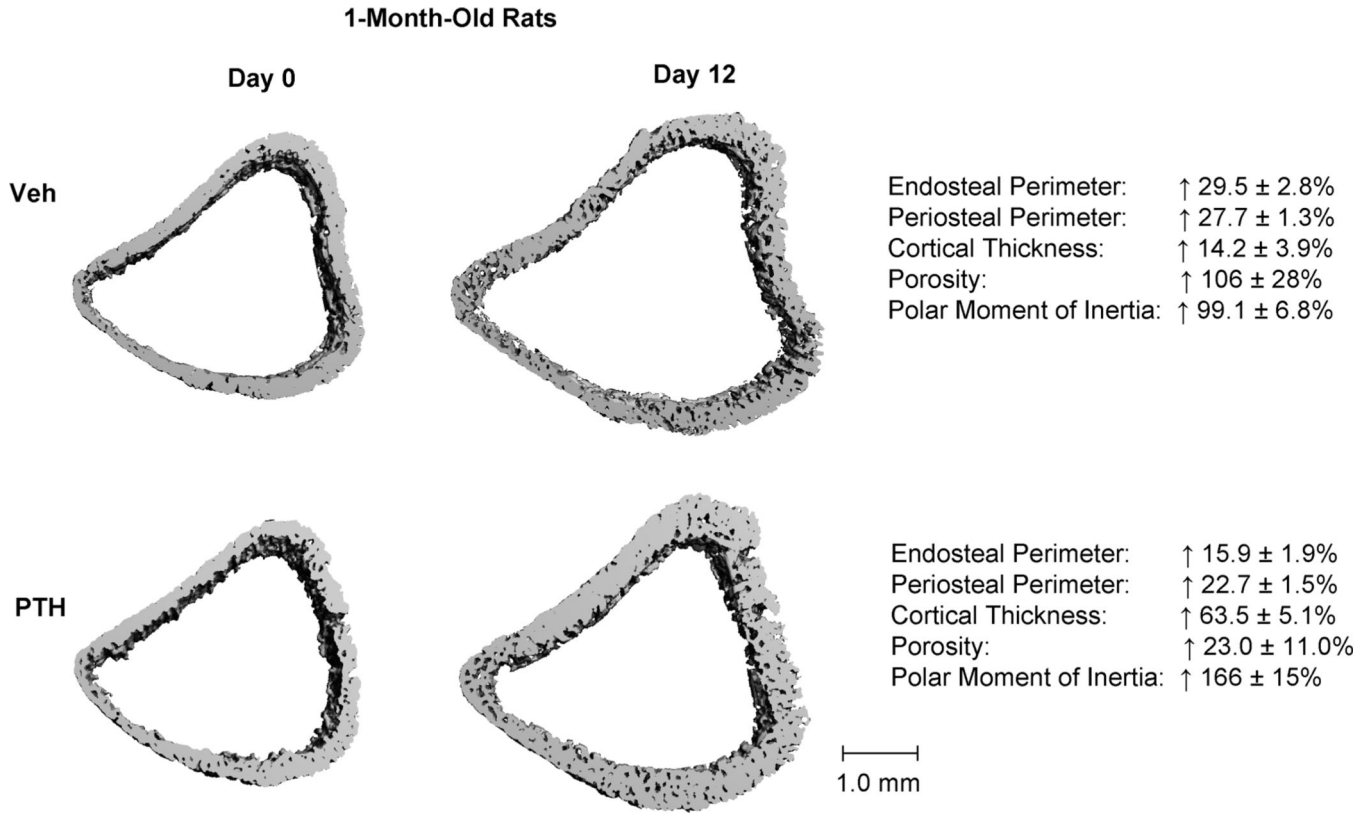


**Figure 5.**

Representative 3D proximal tibia metaphyseal cortical bone images of day 0 (left) and day 12 (right) of Veh- (top) and PTH- (bottom) treated 1-month-old rats. Numbers on right represent percent change over 12 days within each treatment group. All the changes are statistically significant ($p<0.05$).

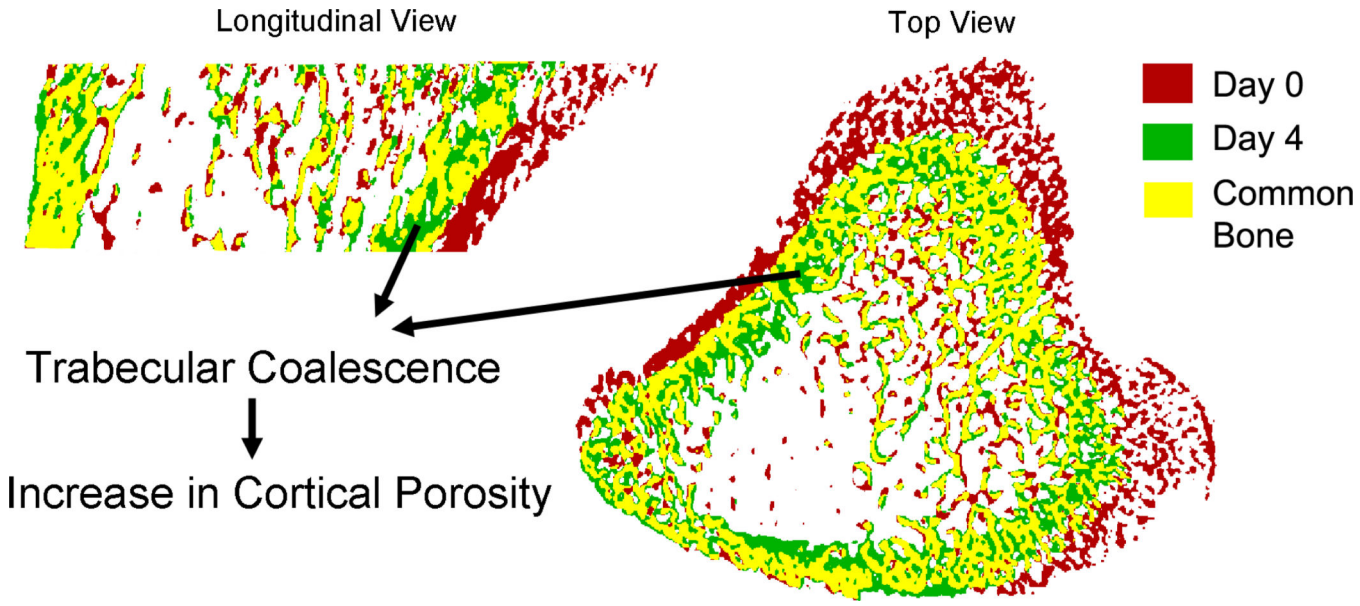


**Figure 6.**

Trabecular coalescence into cortical bone at the proximal tibia metaphysis. The endosteal cortex is formed by trabecular coalescence, leaving unfilled pores between trabeculae, thus increasing cortical porosity during rapid growth.

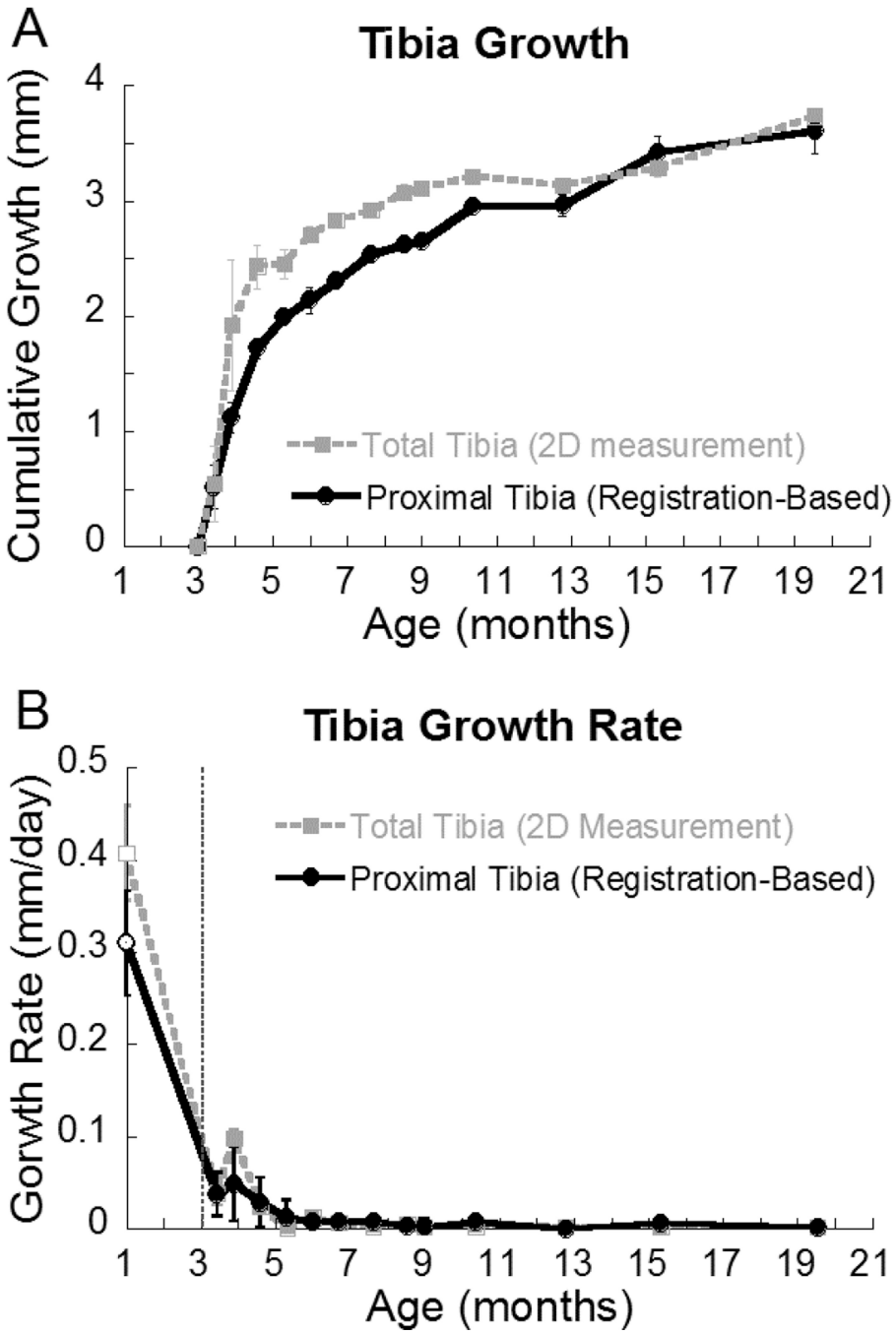


**Figure 7.**

(A) Cumulative growth of the total tibia (derived from 2D scout view) and of the proximal tibia (derived from image registration) after 3-months of age; (B) Growth rate of the total tibia and the proximal tibia. Growth rate at the age of 1-month (empty circle and square) was calculated based on a different set of rats from the growth rate at the age of 3 to 19-month (solid circle and square).

## Table 1

Comparison of trabecular bone structural parameters between day 0 and day 12 of Veh and PTH treated 1-month-old rats. It should be noted that the trabecular bone volume measured at day 12 was newly generated bone tissue due to linear growth.

| 1-month-old rats | Veh | | PTH | |
|---|---|---|---|---|
| | Day 0 | Day 12 | Day 0 | Day 12 |
| Primary Spongiosa | | | | |
| BV/TV | 0.15±0.01 | 0.13±0.01 | 0.17±0.01 | 0.32±0.02 *# |
| Conn.D (1/mm$^3$) | 223±21 | 175±21 | 230±36 | 344±40 *# |
| SMI | 2.19±0.09 | 2.56±0.07 * | 2.20±0.11 | 1.26±0.21 *# |
| Tb.N (1/mm) | 4.89±0.12 | 5.32±0.24 | 5.79±0.28 | 7.61±0.32 *# |
| Tb.Th (mm) | 0.045±0.001 | 0.043±0.001 | 0.045±0.001 | 0.057±0.002 *# |
| Tb.Sp (mm) | 0.21±0.01 | 0.18±0.01 | 0.17±0.01 | 0.11±0.01 *# |
| TMD (mg HA/cm$^3$) | 693±6 | 713±5 * | 727±9 | 751±5 * |
| Secondary Spongiosa | | | | |
| BV/TV | 0.09±0.01 | 0.08±0.01 | 0.10±0.01 | 0.23±0.02 *# |
| Conn.D (1/mm$^3$) | 65.3±12.3 | 40.4±7.0 | 70.4±11.3 | 122.4±15.3 *# |
| SMI | 2.40±0.07 | 2.62±0.08 * | 2.44±0.07 | 1.86±0.11 *# |
| Tb.N (1/mm) | 2.86±0.20 | 3.15±0.13 | 3.32±0.29 | 5.07±0.25 *# |
| Tb.Th (mm) | 0.049±0.002 | 0.049±0.001 | 0.047±0.001 | 0.063±0.001 *# |
| Tb.Sp (mm) | 0.36±0.03 | 0.32±0.01 | 0.32±0.03 | 0.18±0.01 *# |
| TMD (mg HA/cm$^3$) | 787±6 | 770±7 | 793±8 | 792±5 |

Values represented as mean±SEM.

Significant difference between day 0 and day 12 in the same treatment group was indicated by * $p < 0.05$.

In comparing Veh and PTH groups, all parameters were not different at day 0 but some became significantly different (indicated by # $p<0.05$) at day 12.

## Table 2

Comparison of the tibia metaphseal cortical bone parameters between day 0 and day 12 of Veh and PTH treated rats.

| | Veh | | PTH | |
|---|---|---|---|---|
| | **Day 0** | **Day 12** | **Day 0** | **Day 12** |
| The Tibia Metaphyseal Cortex | | | | |
| 1-Month-Old Rats | | | | |
| Ct.En.Pm (mm) | 12.0±0.3 | 15.5±0.2 * | 11.6±0.2 | 13.4±0.3 *# |
| Ct.Pe.Pm (mm) | 13.4±0.3 | 17.1±0.03 * | 13.0±0.2 | 16.0±0.3 *# |
| Ct.Th (mm) | 0.215±0.007 | 0.244±0.005 * | 0.220±0.010 | 0.357±0.012 *# |
| CtpMOI ($mm^4$) | 6.7±0.5 | 13.3±0.9 * | 6.1±0.3 | 16.2±1.1 *# |
| Ct.Po (%) | 14.3±1.9 | 27.0±1.0 * | 15.4±2.1 | 18.6±2.4 # |
| Ct.TMD (mg HA/$cm^3$) | 865±20 | 834±3 * | 877±11 | 864±6 * |
| 3-Month-Old Rats | | | | |
| Ct.En.Pm (mm) | 14.0±0.5 | 14.1±0.7 | 14.0±0.6 | 12.3±0.5 *# |
| Ct.Pe.Pm (mm) | 15.4±0.2 | 15.9±0.5 * | 15.3±0.3 | 15.1±0.3 # |
| Ct.Th (mm) | 0.369±0.016 | 0.388±0.016 | 0.341±0.015 | 0.427±0.021 * |
| CtpMOI ($mm^4$) | 15.8±0.7 | 18.6±1.6 * | 15.1±1.1 | 17.1±1.1 * |
| Ct.Po (%) | 8.63±1.03 | 8.01±0.81 | 8.90±0.56 | 6.99±0.30 *# |
| Ct.TMD (mg HA/$cm^3$) | 1046±16 | 1064±16 * | 1039±11 | 1065±11 * |

Values represented as mean±SEM.

Significant difference between day 0 and day 12 in the same treatment group was indicated by * $p < 0.05$.

In comparing Veh and PTH groups, all parameters were not different at day 0 but some became significantly different (indicated by # $p<0.05$) at day 12.